The Meteoritical Society

Meteoritics & Planetary Science 42, Nr 1, 63–80 (2007)
Abstract available online at http://meteoritics.org

Localized shock melting in lherzolitic shergottite Northwest Africa 1950: Comparison with Allan Hills 77005

E. L. WALTON* and C. D. K. HERD

[1]Department of Earth and Atmospheric Sciences, 1-26 Earth Sciences Building, University of Alberta, Edmonton, Alberta T6G 2E3, Canada
*Corresponding author. E-mail: ewalton@ualberta.ca

(Received 14 June 2006; revision accepted 04 November 2006)

Abstract–The lherzolitic Martian meteorite Northwest Africa (NWA) 1950 consists of two distinct zones: 1) low-Ca pyroxene poikilically enclosing cumulate olivine ($Fo_{70–75}$) and chromite, and 2) areas interstitial to the oikocrysts comprised of maskelynite, low- and high-Ca pyroxene, cumulate olivine ($Fo_{68–71}$) and chromite. Shock metamorphic effects, most likely associated with ejection from the Martian subsurface by large-scale impact, include mechanical deformation of host rock olivine and pyroxene, transformation of plagioclase to maskelynite, and localized melting (pockets and veins). These shock effects indicate that NWA 1950 experienced an equilibration shock pressure of 35–45 GPa. Large (millimeter-size) melt pockets have crystallized magnesian olivine ($Fo_{78–87}$) and chromite, embedded in an Fe-rich, Al-poor basaltic to picro-basaltic glass. Within the melt pockets strong thermal gradients (minimum 1 °C/μm) existed at the onset of crystallization, giving rise to a heterogeneous distribution of nucleation sites, resulting in gradational textures of olivine and chromite. Dendritic and skeletal olivine, crystallized in the melt pocket center, has a nucleation density (1.0×10^3 crystals/mm^2) that is two orders of magnitude lower than olivine euhedra near the melt margin (1.6×10^5 crystals/mm^2). Based on petrography and minor element abundances, melt pocket formation occurred by in situ melting of host rock constituents by shock, as opposed to melt injected into the lherzolitic target. Despite a common origin, NWA 1950 is shocked to a lesser extent compared to Allan Hills (ALH) 77005 (45–55 GPa). Assuming ejection in a single shock event by spallation, this places NWA 1950 near to ALH 77005, but at a shallower depth within the Martian subsurface. Extensive shock melt networks, the interconnectivity between melt pockets, and the ubiquitous presence of highly vesiculated plagioclase glass in ALH 77005 suggests that this meteorite may be transitional between discreet shock melting and bulk rock melting.

INTRODUCTION

The Martian meteorite Northwest Africa (NWA) 1950, comprised of two stones weighing 414 and 383 g, was recovered from an unknown location in the Atlas Mountains of Morocco in 2001 (Russell et al. 2004). NWA 1950 is one of seven lherzolitic shergottites: Allan Hills (ALH) 77005 (McSween et al. 1979), Lewis Cliff (LEW) 88516 (Gleason et al. 1997), Yamato (Y-) 793605 (Ikeda 1997), Grove Mountain (GRV) 99027 (Hsu et al. 2004), GRV 020090 (Russell et al. 2005), and NWA 2646 (Bunch et al. 2005), representing the first sample of this type recovered outside of Antarctica. NWA 1950 was originally described as a plagioclase-bearing ultramafic cumulate rock consisting of olivine, low- and high-Ca pyroxene, and plagioclase (transformed to maskelynite by shock metamorphism) (Russell et al. 2004). Based on petrologic observations (e.g., Mikouchi 2005), the crystallization sequence for NWA 1950 involves: 1) accumulation of olivine and chromite, 2) crystallization of low-Ca pyroxene poikilitically enclosing cumulus olivine and chromite with low-Ca pyroxene zoning compositionally to augite during growth as oikocrysts, 3) continued crystallization of intercumulus liquid as plagioclase, pigeonite, ilmenite, and whitlockite associated with re-equilibration of cumulus olivine, and 4) late-stage reaction of chromite, where it is in contact with interstitial liquid, to form titanium-rich chromite. The bulk rock oxygen isotopic composition, $\delta^{17}O = 2.54‰$, $\delta^{18}O = 4.28‰$, and $\delta^{17}O = 0.312‰$ (Gillet et al. 2005), plot on the fractionation line defined by other Martian meteorites, confirming a Martian origin. The $\delta^{18}O$ signature is indistinguishable from the other lherzolitic shergottites (Clayton and Mayeda 1996; Franchi et al. 1999). Cosmic-ray exposure (CRE) ages for NWA 1950, based on stable noble gas isotopes ^{38}Ar, ^{21}Ne, and ^{3}He, are 2.3

© The Meteoritical Society, 2007. Printed in USA.

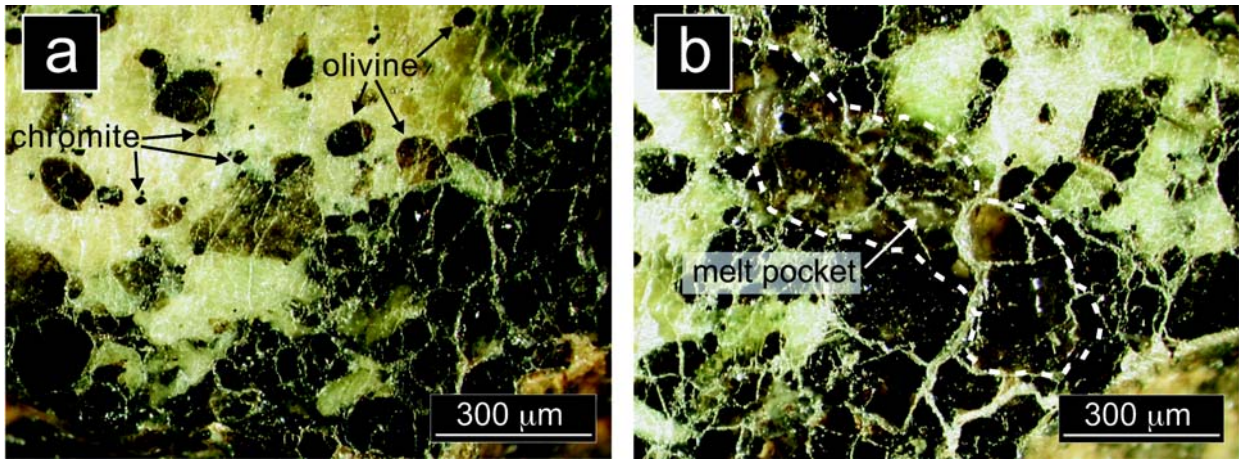


Fig. 1. Reflected light images of the NWA 1950 sample investigated in this study. a) Interpenetrating light (top left) and dark (bottom right) areas. b) Pockets of shock melt material (outlined by cross hatching) appear cloudy in reflected light, crosscutting both light (top right) and dark (bottom) igneous areas.

± 1.0 Myr, 3.5 ± 0.8 Myr, and 5.3 ± 3.0 Myr, respectively (Gillet et al. 2005). The reported CRE ages span those previously reported for other lherzolitic shergottites: 2.5–3.4 Myr for ALH 77005 (Bogard et al. 1984; Nishiizumi et al. 1986; Pal et al. 1986; Miura et al. 1995; Eugster et al. 1996); 3.0–4.1 Myr for LEW 88516 (Treiman et al. 1994; Eugster et al. 1996); and 3.9–5.4 Myr for Y-793605 (Terribilini et al. 1998; Eugster and Polnau 1997; Nagao et al. 1997, 1998). This spread in CRE ages (2.3–5.4 Myr) may be the result of a complex exposure history, including a contribution from solar cosmic rays (Gillet et al. 2005) or irradiation by cosmic rays at the surface of Mars (Nagao et al. 1997).

NWA 1950 exhibits bulk shock effects (mechanical deformation, formation of diaplectic glass), localized melt features (melt veins and pockets), and friction melts (shock veins). These features are typical of Martian shergottites (basaltic, olivine-phyric basaltic, and lherzolitic), presumably formed during the impact event, which launched the rocks into eventual Earth-crossing trajectories from the Martian near-surface. The mechanism and physical conditions required to launch Martian surface or near surface rocks at velocities in excess of 5.0 km/s (Martian escape velocity; Wetherill 1984), are investigated theoretically by numerical modeling (Head et al. 2002; Artemieva and Ivanov 2004). The predictions of these models can only be evaluated by studying the physical imprint of this impact event on the material ejected. Currently, there exist 34 unpaired samples of ejected Martian material in the world's meteorite collection (Meyer 2006). The increase in Martian meteorite recovery, 22 in the last decade, coupled with the likelihood of an eventual Martian sample return mission, requires comprehensive descriptions of Martian samples to keep the database current as new meteorites are recovered (see Meyer 2006).

Here we present a detailed study of the petrology and mineralogy of localized shock-generated melt pockets in NWA 1950 with implications for its impact history, and evaluation of its relationship to ALH 77005 in terms of shock metamorphism. New data on mineral compositions are also reported. NWA 1950 exhibits shock metamorphic features distinct from those observed in ALH 77005 in terms of modal abundance, mineralogy, and internal microtextures. Comparison of shock metamorphic features, when combined with current models for Martian meteorite ejection, may help to shed light on mechanisms responsible for their formation.

ANALTYICAL METHODS

Two doubly polished thick sections, NWA 1950 (2.6 g; ~2.1 cm × 1.0 cm × 0.2 cm) and ALH 77005 (0.2 g; 1.0 cm × 0.3 cm × 0.2 cm), and one polished thin section (PTS) of ALH 77005 (ALH 77005,122) were initially studied by reflected, plane and transmitted (PTS only) light microscopy. Backscattered electron (BSE) and secondary electron (SE) images were obtained using a JEOL 6301F Field Emission (FE) SEM at a working distance of 8 mm and an accelerating voltage of 20 kV. Minerals and glasses were analyzed using a JEOL 8900 electron microprobe (EM) equipped with five wavelength dispersive spectrometers (WDS) using an accelerating voltage of 15 or 20 kV and a beam current of 15 or 20 nA. Glasses were analyzed using a defocused beam (3–10 μm diameter). Natural minerals were used as standards for all EM analyses. Mineral modes for major phases were determined by manual point counts on BSE images. Mineral/glass modes for melt pockets are based on visual estimates. The image analysis software, ImageJ, was used to determine the nucleation density of NWA 1950 melt pockets.

PETROGRAPHY

NWA 1950 is a plagioclase-bearing ultramafic cumulate rock. In hand specimen NWA 1950 exhibits interpenetrating light and dark areas, typical of lherzolitic shergottites (e.g.,

Harvey et al. 1993; Treiman et al. 1994; Lin et al. 2005) (Fig. 1). Microscopic investigation reveals that NWA 1950 is comprised of three distinct textures: poikilitic (dark) crystalline, interstitial or non-poikilitic (light) crystalline and glassy to partially crystalline pockets and veinlets. Melt pockets are dispersed heterogeneously throughout NWA 1950, crosscutting igneous textures, and are observed in both poikilitic and interstitial areas (for details, see the Shock Metamorphism section).

In poikilitic areas, millimeter-size (up to ~5 mm) low-Ca pyroxene grains poikilitically enclose rounded olivine (80–1100 μm; avg. 450 μm) and chromite euhedra (8–110 μm; avg. 35 μm). Maskelynite is rarely observed in this texture. Non-poikilitic areas are interstitial to the large pyroxene oikocrysts and have basaltic textures of subrounded olivine (90–575 μm; avg. 200 μm), anhedral low- and high-Ca pyroxene (60–400 μm; avg. 140 μm), maskelynite laths (after plagioclase, 14–470 μm; avg. 130 μm) and chromite euhedra (10–105 μm; avg. 32 μm). Trapped multiphase magmatic inclusions (Al-Ti-rich pyroxene and Si-rich feldspathic glass) are observed in olivine in both poikilitic and interstitial zones. Whitlockite, ilmenite, Fe sulfide, and rare baddeleyite are generally restricted in occurrence to non-poikilitic areas. The boundary between poikilitic/non-poikilitic is not obvious in SEM images, nor is it clearly delineated in X-ray maps.

The mineral mode (in vol%), determined by manual point counting (n = 3000; ~2.1 cm^2), is 45.3% olivine, 34.5% pyroxene (high- and low-Ca), 11.0% maskelynite, 5.7% chromite, 1.8% melt pockets and 1.7% primary melt inclusions in olivine (Table 1). These results are in good agreement with the mineral modes reported by Gillet et al. (2005).

SHOCK METAMORPHISM

NWA 1950 is an unbrecciated meteorite, recording petrographic evidence for a single shock history similar to other Martian meteorites, with the exception of monomict breccias ALH 84001 and Yamato-793605 (Mittlefehldt 1994; Ikeda 1997). Shock veins, thin (1–100 μm) glassy veins that transect the entire sample, displacing and truncating host rock minerals, are reported from the NWA 1950 thin section examined by Mikouchi (2005). Shock veins have not been observed in the sample investigated in this study. This may be an artefact of the two-dimensional nature of the sample, coupled with the low volume proportion of shock melting in this meteorite (see the Petrography section).

Shock Recorded in the Bulk Rock

Bulk shock effects are defined here as any change in host rock minerals, recorded throughout the bulk sample, as a result of shock metamorphism. In NWA 1950, evidence for strong shock metamorphism of the bulk sample is revealed by the complete transformation of plagioclase to maskelynite (diaplectic plagioclase glass) with no relict birefringence (see Gillet et al. 2005 for Raman spectra), a high degree of irregular fractures and strong mosaicism observed in olivine and pyroxene (low- and high-Ca), and multiple sets of planar fractures in olivine grains. Gillet et al. (2005) report Raman spectra of heavily distorted olivine, which show an additional band near 750 cm^{-1} suggesting the local formation of Si-O-Si bridges. This is typical of wadsleyite, $(Mg,Fe)_2SiO_4$, a high-pressure high-temperature polymorph of olivine. The presence of wadsleyite indicates a minimum pressure and temperature regime of 14 to 15 GPa (Katsura et al. 2004; reported for Mg_2SiO_4 between 1327 and 1627 °C). In polarized transmitted light, wadsleyite can be identified by a bluish-grey color, while the other high pressure polymorph of olivine, ringwoodite, has a distinctive purple color (e.g., Mason et al. 1968; Colemann 1977). The presence of ringwoodite or wadsleyite could not be determined from the thick sections investigated in this study, however, Mikouchi et al. (2005) and Gillet et al. (2005) did not observe any such unusually colored olivine in the NWA 1950 thin sections they studied. Maskelynite displays radiating fractures that extend from grain margins into neighboring host rock minerals. Normal plagioclase glass, characterized by flow-structured schlieren and vesiculation, is manifest as minor grain boundary melting, and is subordinate in abundance to that of diaplectic glass. Diaplectic glass is optically isotropic, preserving the original shape of the precursor plagioclase grain with no evidence for flow or vesiculation, distinguishing it from normal glass of plagioclase-composition. Typically, grain boundary melting is associated with melt pockets, discussed in the following section. Opaque phases (chromite, ilmenite), contain irregular fractures and microfaulting with μm offsets observed in several grains.

Localized Shock Melting

In cross section, melt pockets occur as small, 60–200 μm size subrounded enclaves, typically developed at grain boundaries (chromite-pyroxene, plagioclase-olivine-pyroxene; Fig. 2), and large millimeter-size (up to 1.4 mm in the longest dimension) irregularly shaped, enclaves that obscure original grain boundaries (Fig. 3). These localized regions of melting occupy up to 1.8% of NWA 1950 by volume (Table 1) and are self-contained, at least within the two dimensions of the thin section (i.e., no compound, interconnected, or overlapping melt pockets were observed). SEM BSE investigation reveals that melt pockets are complex mixtures of varying proportions of silicate crystallites + glass + host rock clasts + vesicles/vugs.

Small melt pockets typically have a glassy groundmass with flow-textured schlieren containing blebs of immiscible sulfides, stringers of chromite, crystallites (1–8 μm), and clasts of host rock minerals. Entrained clasts have reacted

Table 1. Compiled data for modal phase abundance and equilibration shock pressure of Martian meteorites.

Meteorite	Nakhlite[a]	Y-980459[b]	Zagami[c]	NWA 1950	Los Angeles[c]	SaU 150[d]	DaG 476[c]	LEW 88516[e]	ALH 77005[e]		
				Tile						PTS	Tile
Pyroxene (total)	65–85.2	52.6	70.6	34.5	38.4	49.8–54.6	50.2	37.3	13.2	26.9	11.6
Olivine	2–20	15.7	n.p.	45.3	n.p.	17.2–23.1	18.2	45.9	60.2	45.9	42.9
Maskelynite	n.p.	n.p.	24.8	11.0	39.5	13.8–15.5	19.4	7.0	9.5	7.4	11.4
Opaques[f]	n.a.	31.7	2.4	5.7	14.3	1.6–3.8	2.1	1.6	4.0	5.2	3.4
Phosphates	n.a.	n.p.	0.6	n.a.	n.a.	tr	tr	0.9	0.4	n.a.	n.a.
Melt inclusions	n.a.	0.1	n.a.	1.7	n.a.	0.2–0.3	n.a.	n.a.	n.a.	1.6	1.5
Mesostasis	4.7–35	n.p.	n.p.	n.p.	n.p.	n.p.	n.p.	n.p.	n.p.	n.p.	n.p.
Shock melt	n.p.	tr	2.2	1.8	7.8	10.2–11.3	10.1	7.7	13.7	12.9	29.2
ESP[g] (GPa)	5–20	20–25	29.5 ± 0.5	35–45	45 ± 3	40–45	40–45	43 ± 3	45–55		

[a]Compiled by Meyer (2006).
[b]Mikouchi et al. (2004).
[c]Walton et al., Forthcoming.
[d]Walton et al. (2005).
[e]Treiman et al. (1994).
[f]Mineral/phase opaque in transmitted light, i.e., chromite, ilmenite, pyrrhotite, glass (Y-980459), and vermicular intergrowth (silica + hedenbergite + fayalite; Los Angeles).
[g]ESP: equilibration shock pressure in gigapascals (GPa) from Fritz et al. 2005 (Y-980459 from Greshake et al. 2004).
n.a. = not analyzed; n.p. = mineral/phase not present in meteorite; tr = trace abundance <0.1 vol%; Tile = thick section (this study, surface area for NWA 1950 ~2.1 cm^2; ALH 77005 ~0.3 cm^2); PTS = polished thin section (this study, ALH 77005,122; surface area ~1.2 cm^2).

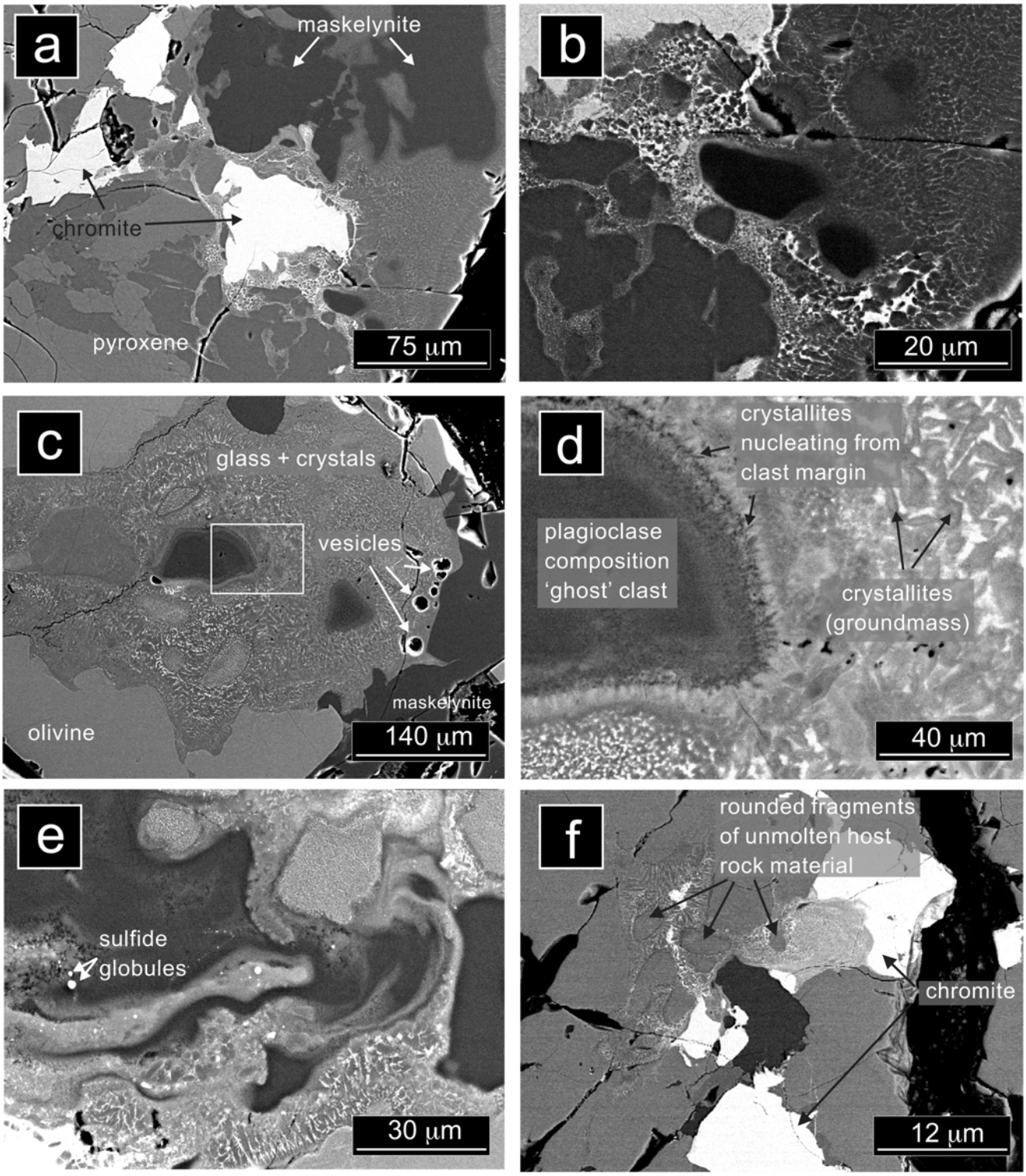


Fig. 2. BSE images of melt pockets in NWA 1950. a) Small melt pocket defined by remobilized chromite (stringers and veins) and maskelynite/plagioclase glass with diffuse boundaries intermingling with pyroxene. b) Higher magnification of melt pocket depicted in (a). c) Subrounded melt pocket at the grain boundary between olivine and maskelynite. Groundmass crystallites and internal texture of relict host rock fragments entrained within the melt are shown at higher magnification in (d). e) Schlieren-rich melt pocket with sulfide globules. f) Irregularly shaped melt pocket occurring adjacent to chromite, maskelynite, and olivine in the host rock.

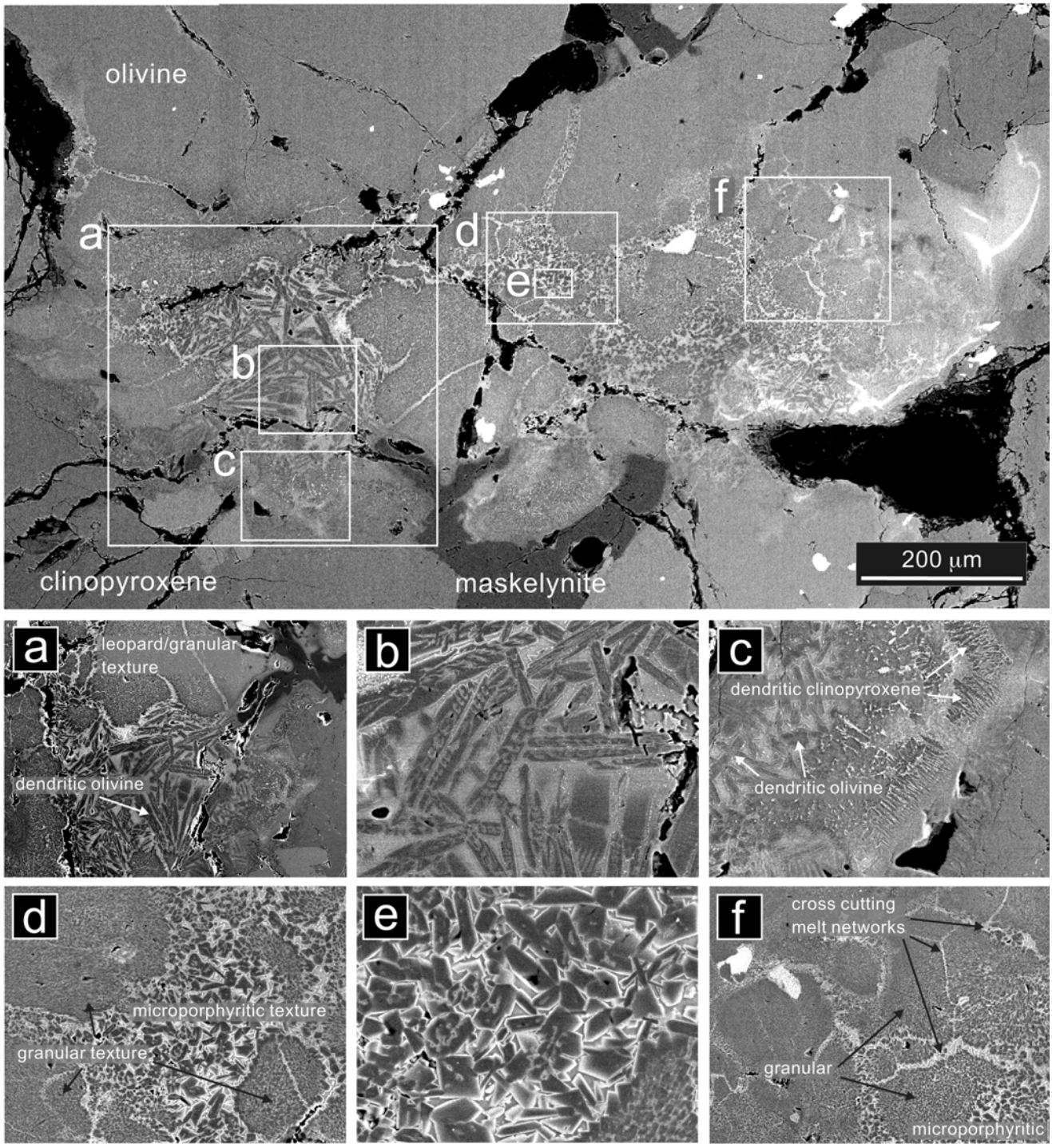


Fig. 3. BSE image mosaic of a large melt pocket in NWA 1950. The letters indicate the corresponding BSE image, located below the melt pocket overview, taken at higher magnification and rotated 90° CCW.

with the melt to varying degrees. Crystallites, ~1 μm in size, nucleate from the edge of clasts into the melt pocket. Chromite has been remobilized to fill the cracks and fractures of adjacent host rock minerals (pyroxene, olivine). Maskelynite, in contact with small melt pockets, has diffuse boundaries containing flow textures (normal plagioclase glass) and vesicles, coexisting and intermingling with partially melted olivine and pyroxene.

Larger melt pockets have crystallized olivine, chromite and clinopyroxene, exhibiting a range of crystal shapes, embedded in silicate glass with minor subrounded vesicles and irregular vugs. Partially crystallized melt material,

emanating from the main melt pocket, crosscuts host rock olivine and pyroxene. These melt veins are typically interconnected, surrounding unmolten host rock constituents. Host rock minerals and melt pockets display gradational textures approaching the melt/host rock margin. Within the host rock, single crystal (igneous) olivine gives way to a recrystallized, granular zone of anhedral, irregular olivine crystals with no mesostasis as the melt pocket is approached. This granular zone varies in apparent thickness from tens to hundreds of microns (up to 250 μm). Closer to the melt pocket (10–20 μm) olivine likewise shows a recrystallized granular texture, however, the crystal shape changes to equant, euhedral olivine crystals (2–8 μm in size, with no mesostasis). Grain boundaries between granular olivine crystals in this zone form a triple point junction. Progressing from this recrystallized zone into the melt pocket, the texture changes from granular to microporphyritic (equant, euhedral olivine crystals too fine-grained to be visible to the unaided eye, 3–25 μm in size, set in a glassy matrix; ~95% crystals, ~5% glass). In the melt pocket interior (~150 μm into the melt pocket from the margin), the texture remains microporphyritic, however, the olivine crystal shape changes to dendritic (branching and chain; Donaldson 1976; Faure et al. 2003), associated with an increase in the proportion of mesostasis glass (~70% crystals with apparent size 32–114 μm length, 4–14 μm width; ~30% glass). These progressive textures, from melt pocket margin to interior, are illustrated in Fig. 3.

Chromite also displays gradational textures from melt pocket margin to center. Chromite, entrained within the melt pocket, near the margin (tens of microns) has reacted with the melt forming a mottled, recrystallized texture retaining the overall shape of the original chromite grain (Fig. 4). Several recrystallized grains exhibit a frothy, vesiculated internal texture (Fig. 4). Mottled, recrystallized chromites are lacking in the center of the melt pocket. Small (1–3 μm in size) chromite euhedra and dendrites are disseminated throughout the melt pocket. Clinopyroxene, in direct contact with the melt pocket, shows flow lines and intermingles with partially melted olivine and plagioclase glass. Fine clinopyroxene dendrites (6–10 μm in length, 1–2 μm in width) nucleate from the margin of host rock clinopyroxene. Clinopyroxene dendrites are restricted in occurrence to the host rock clinopyroxene/melt margin; olivine is the dominant phase to crystallize in the melt pocket interior. Maskelynite in direct contact with the melt pocket shows diffuse boundaries and intermingles with stringers and blebs of silicate glass from the melt pocket.

MINERAL COMPOSITION

Olivine enclosed by low-Ca pyroxene in poikilitic areas shows little compositional variation ($Fo_{70–75}$) and is more magnesian than olivine in non-poikilitic areas ($Fo_{68–71}$). Core compositions of olivine microphenocrysts (those crystallized from melt pockets), are more magnesian than olivine in poikilitic and nonpoikilitic areas (cumulate olivine), as well as granular olivine adjacent to the melt pocket (within the host rock), ranging from $Fo_{78–87}$. Olivine microphenocrysts, and granular olivine, are strongly zoned, although the small grain size inhibits quantitative analyses. For olivine microphenocrysts, analyses closer to the rim show less magnesian compositions, ranging from $Fo_{49–59}$; however, the rims of granular olivine are never as Mg-poor (core $Fo_{70–72}$, rim $Fo_{66–69}$), lying close to the compositional range observed in cumulate olivine ($Fo_{68–75}$). This strong zoning gives granular olivine a distinctive leopard pattern (Fig. 3). The interstitial glass of the melt pockets has an Fe-rich (23.25–30.23 wt% FeO), Al-poor (3.87–5.95 wt% Al_2O_3) basaltic to picro-basaltic composition.

These olivine types (cumulate versus olivine recrystallized to varying degrees during a later thermal event) are easily distinguished on a plot showing variation in minor element abundance as a function of mg-number (atomic Mg/Mg + Fe × 100) (Fig. 5). MnO in melt pocket olivine falls along the same trend as cumulate and granular olivine, decreasing with increasing mg-number, attributable to the incompatible nature of Mn in olivine. Cr_2O_3 abundances in cumulate olivine are low (0.01–0.16 wt% Cr_2O_3), compared to granular olivine, which exhibits steep, near vertical Cr_2O_3 abundances at higher mg-numbers (69–71). Cr_2O_3 abundances in olivine crystallized from melt pockets are much higher (0.3–1.0 wt%). Although the results are more scattered than reported for MnO, Cr_2O_3 generally increases with increasing mg-number with near vertical trends at the highest mg-numbers ($Fo_{83–87}$) and a slight downturn in Cr_2O_3 from the Mg-poor crystallite rim ($Fo_{49–58}$).

Olivine grains entrained within the melt pocket have reacted with the shock melt. They are characterized by the granular "leopard" texture, described for host rock olivine in direct contact with the melt pocket. Olivine euhedra nucleate from the relict clast margin into the melt pocket groundmass. The composition ($Fo_{68–72}$) overlaps with that of granular olivine from the melt pocket margin and cumulate olivine.

Host rock and melt pocket chromite compositions in NWA 1950 are compared in Fig. 6. Chromite compositions in the NWA 1950 host rock are very similar to those in ALH 77005 (e.g., as described by Goodrich et al. 2003): chromites enclosed by pigeonite or olivine in the poikilitic areas are low in Ti, and show variation in Cr-Al; chromites enclosed by olivine are more aluminous; and chromites in non-poikilitic areas vary continuously in ulvöspinel content, Usp = 5–60%, where Usp = molar $2Ti/(2Ti + Cr + Al + Fe^{3+})$. The main difference is reflected by the Cr# (= molar Cr/(Cr + Al)) of the chromite: NWA 1950 chromites extend to Cr# = 0.93, whereas ALH 77005 chromites have Cr# < 0.90 (see ALH 77005 mineral composition in the Discussion section; Goodrich et al. 2003). The compositions of the mottled, recrystallized chromite grains near the melt pocket margins in

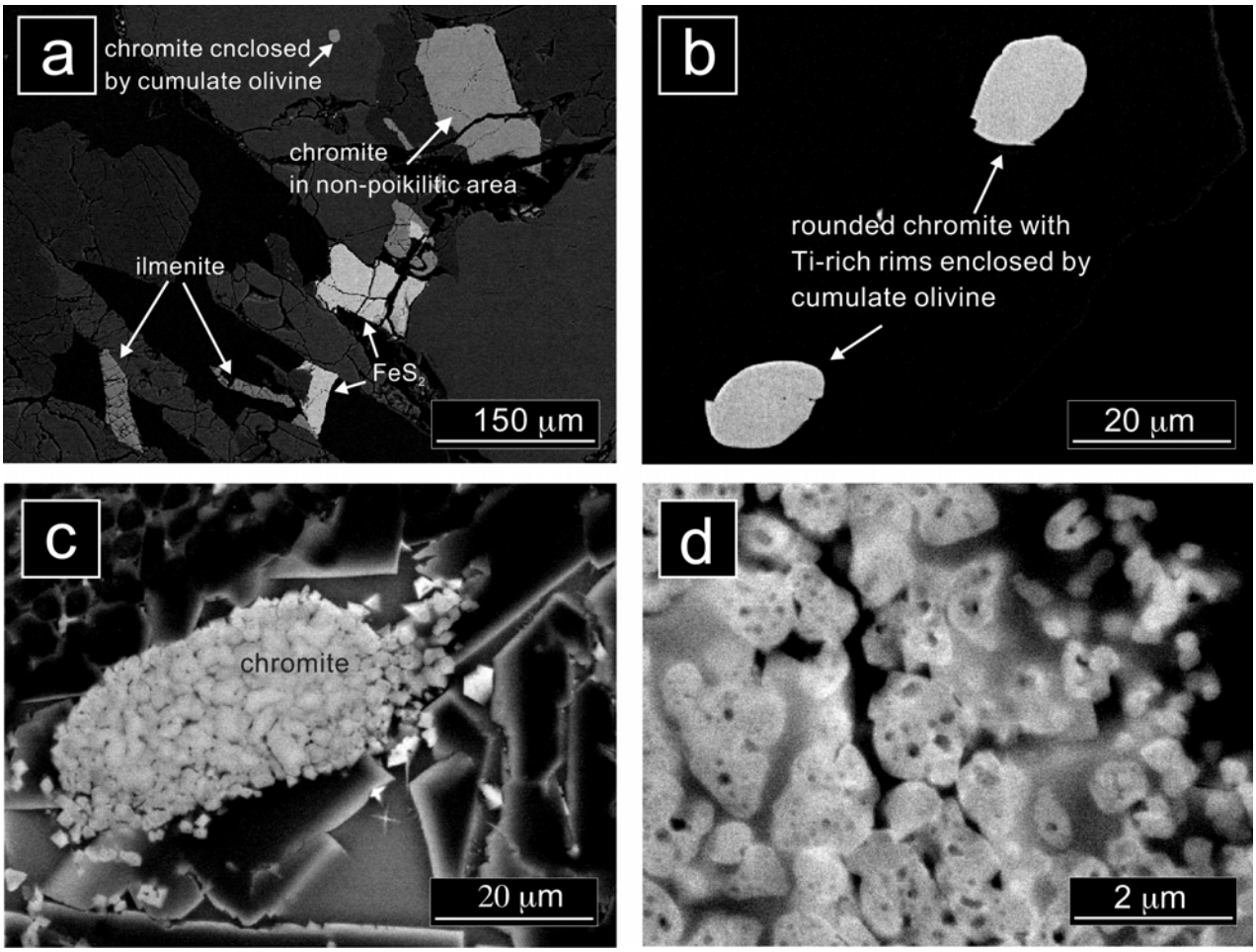


Fig. 4. BSE images showing the various chromite textures in NWA 1950. a) Ilmenite + FeS_2 + chromite in a non-poikilitic area. Chromite grains enclosed by cumulate olivine have rounded shapes. b) Higher magnification of chromite inclusions in cumulate olivine showing their rounded shapes and Ti-rich rims. c) Chromite within melt pockets retains the overall shape of the original grain, however, the internal texture has changed from homogeneous (igneous) to polycrystalline. d) Frothy, vesiculated chromite within the melt pocket.

NWA 1950 generally overlap the compositions of chromite grains in the host rock (Fig. 6), indicating that they have retained the composition of the original chromite grains before shock.

DISCUSSION

Shock Features in Allan Hills 77005

ALH 77005 is the most strongly shocked Martian meteorite recovered to date (45–55 GPa; Fritz et al. 2005). Throughout the bulk rock, olivine and pyroxene display planar microdeformation features, strong mosaicism, and lens-shaped deformation bands (olivine only). Olivine exhibits a brown color, which has been attributed to shock oxidation of this phase (Ostertag et al. 1984), as supported by experimental results at shock pressures above 44 to 56 GPa (Reimold and Stöffler 1978; Bauer 1979). However, similar brown to black olivine in the NWA 2737 chassignite has been attributed to nano-scale iron metal and/or transformation to wadsleyite (Beck et al. 2006; Reynard et al. 2006; Treiman, personal communication). High pressure polymorphs of olivine (ringwoodite, wadsleyite), identifiable in thin section by a distinct purple to bluish-gray color in polarized transmitted light, have not been identified in this study, nor are they reported in previous studies of ALH 77005 (e.g., Boctor et al. 1998). Strongly vesiculated plagioclase glass is ubiquitous in the host rock, typically rimmed by birefringent plagioclase with undulatory extinction (2–8 μm in width). Flow structures have been observed in some of the plagioclase glass, increasing in volume with proximity to the melt pockets.

Localized melt features (veins and pockets) are a major component of ALH 77005 (13 to 30 vol%; Table 1). Melt pockets range in apparent diameter from 200–6500 μm. Host rock minerals adjacent to melt pockets show an increase in the intensity of microdeformation (planar fractures, mosaicism) giving way to a zone of recrystallization within a

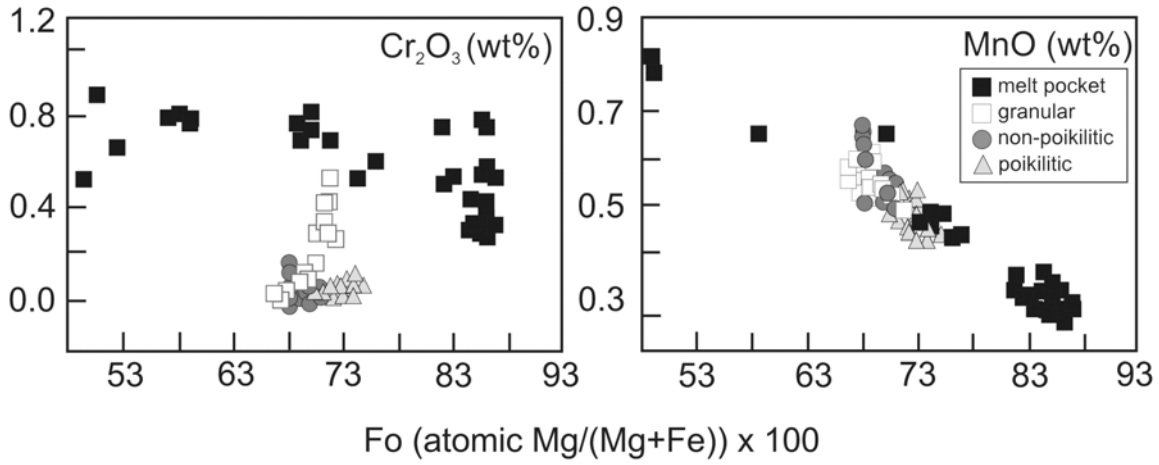


Fig. 5. Variations of Cr_2O_3 and MnO, relative to mg-numbers, in cumulate olivine (poikilitic and non-poikilitic), recrystallized olivine adjacent to melt pocket (granular) and melt pocket crystallites (melt pocket) from NWA 1950.

few hundred microns (up to 300 μm) distance to the melt pocket margin. The progressive change in texture from single crystal to melt pocket is similar to that described for NWA 1950: granular olivine texture progressing to microporphyritic, marking the melt pocket margin. Dendritic and elongate skeletal crystal shapes are typically observed in the melt pocket interior, although several melt pockets are dominated by olivine euhedra with minor hopper crystal shapes (Fig. 7). Microphenocrysts are olivine, zoned to Fe-rich compositions at the rim, with minor clinopyroxene and chromite dendrites. Clinopyroxene is typically observed as fine, feathery crystallites dispersed throughout the melt pocket groundmass (glass), interstitial to olivine microphenocrysts. Chromite shows gradational textures, dependent on distance from the melt pocket contact with the host rock (Fig. 8). Within tens of microns of the contact, the edges of chromite grains have a recrystallized texture grading to a relatively homogeneous core. With distance from the contact toward the melt pocket center, the internal texture becomes completely recrystallized, retaining the overall shape of the original grain. Near the melt pocket center, chromite becomes increasingly disseminated until the original grain shape is no longer recognizable. At this point chromite occurs as minute (1–2 μm) euhedra and dendrites.

Veins (10–75 μm apparent diameter) of partially crystallized melt material emanate from the main melt pocket, crosscutting host rock minerals. The relationship between melt veins and host rock minerals shows a variety of textures. Melt veins have been observed to: 1) interconnect, isolating unmolten host rock constituents, 2) have a wedge shape, tapering off with <200 μm distance from the melt pocket, and 3) enlarge to form subsidiary melt pockets (Fig. 9).

Shock veins occur as thin black, glassy veins (apparent diameter <10 μm), which transect the entire sample as straight, or slightly curved, dikelets having sharp contacts with host rock minerals (Fig. 7). Displacement and truncation

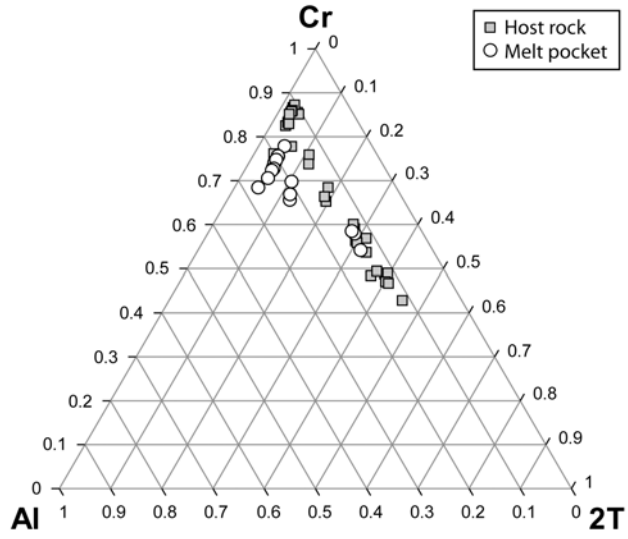


Fig. 6. Compositions of chromites in NWA 1950 in the system chromite (molar Cr/[Cr + 2Ti + Al])-ulvöspinel (molar 2Ti/[Cr + 2Ti + Al])-spinel (molar Al/[Cr + 2Ti + Al]). Melt pocket compositions are those of mottled, recrystallized chromites near melt pocket margins.

of neighboring host rock phases indicates a frictional component to their formation. These shock veins have not been observed to emanate from, or connect to, melt pockets. The texture and context of shock features recorded in the bulk rock and regions of localized melting are illustrated in Figs. 7, 8, and 9.

Allan Hills 77005 Mineral Compositions

Olivine grains analyzed for ALH 77005 show the same general trends as NWA 1950 olivine; for example, olivine poikilitically enclosed by low-Ca pyroxene is more magnesian ($Fo_{70–74}$) compared to olivine in non-poikilitic

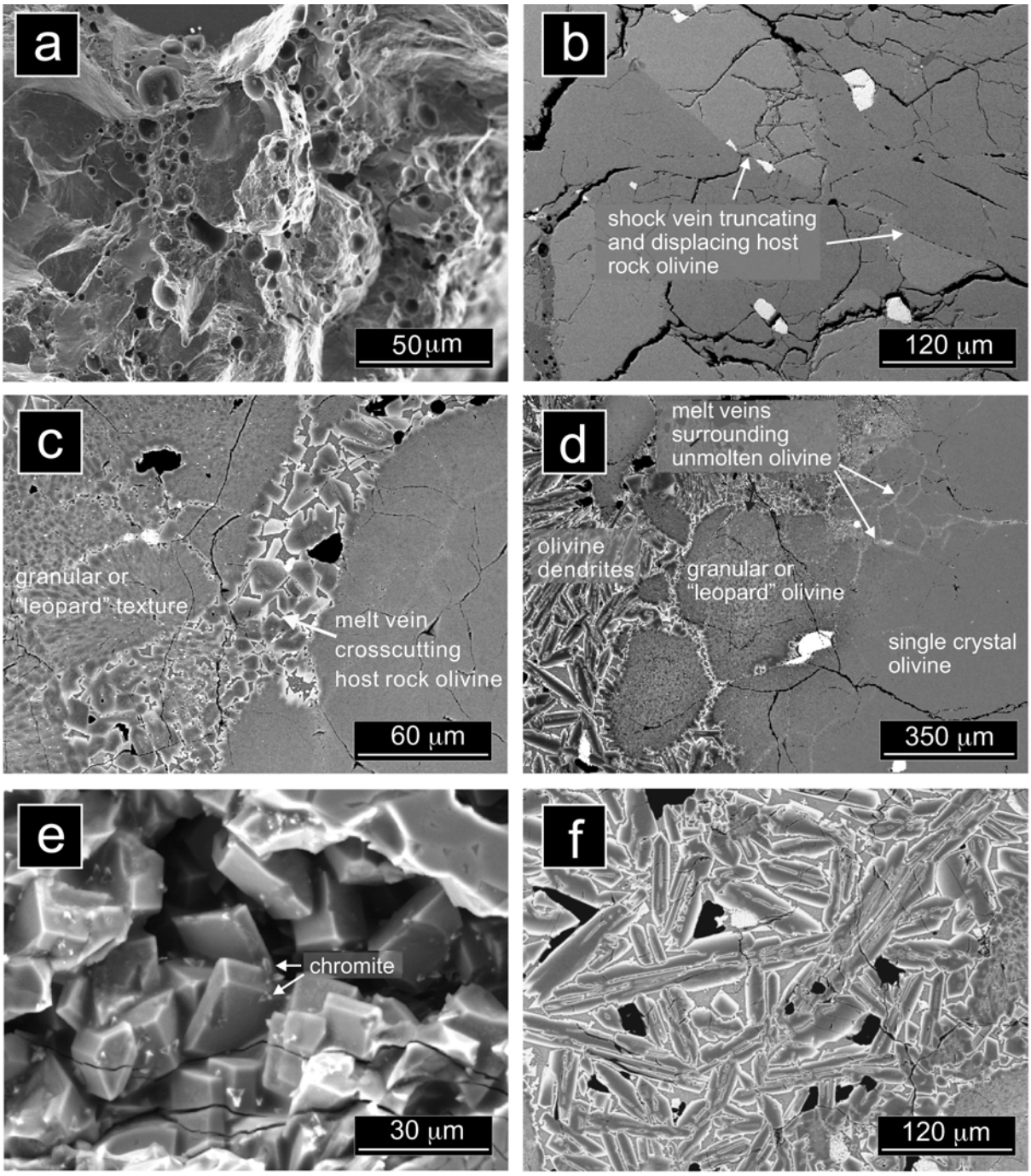


Fig. 7. FEG-SEM images of shock effects in ALH 77005. a) Strongly vesiculated plagioclase glass ubiquitous in the host rock. b) A shock vein truncates and displaces host rock olivine. c) Melt vein truncating host rock olivine. d) Transition from host rock (right) to melt pocket (left). e) Prismatic olivine in a melt pocket. f) Melt pocket containing zoned elongate skeletal olivine embedded in glass. Images (a) and (e) are SE images, and (b), (c), (d), and (f) are BSE images.

areas ($Fo_{68–72}$). In contrast, however, data from ALH 77005 span a wider range of mg-numbers, as a result of the melt pocket microphenocrysts, which have magnesian cores ($Fo_{71–89}$). The outer 1–2 microns are strongly zoned to Fe-rich compositions. In general, analyses closer to the rim yield a range in Mg contents from $Fo_{35–57}$. The glassy matrix to the melt pockets contains feathery clinopyroxene crystals and minute chromite inclusions. The interstitial glass has an Fe-rich (12.65–13.98 wt% FeO), Al-poor (8.43–9.89 wt% Al_2O_3) basaltic to basaltic andesitic composition. Analyses from melt pocket crystallites are distinguished based on minor element abundances and mg-number (Fig. 10). MnO

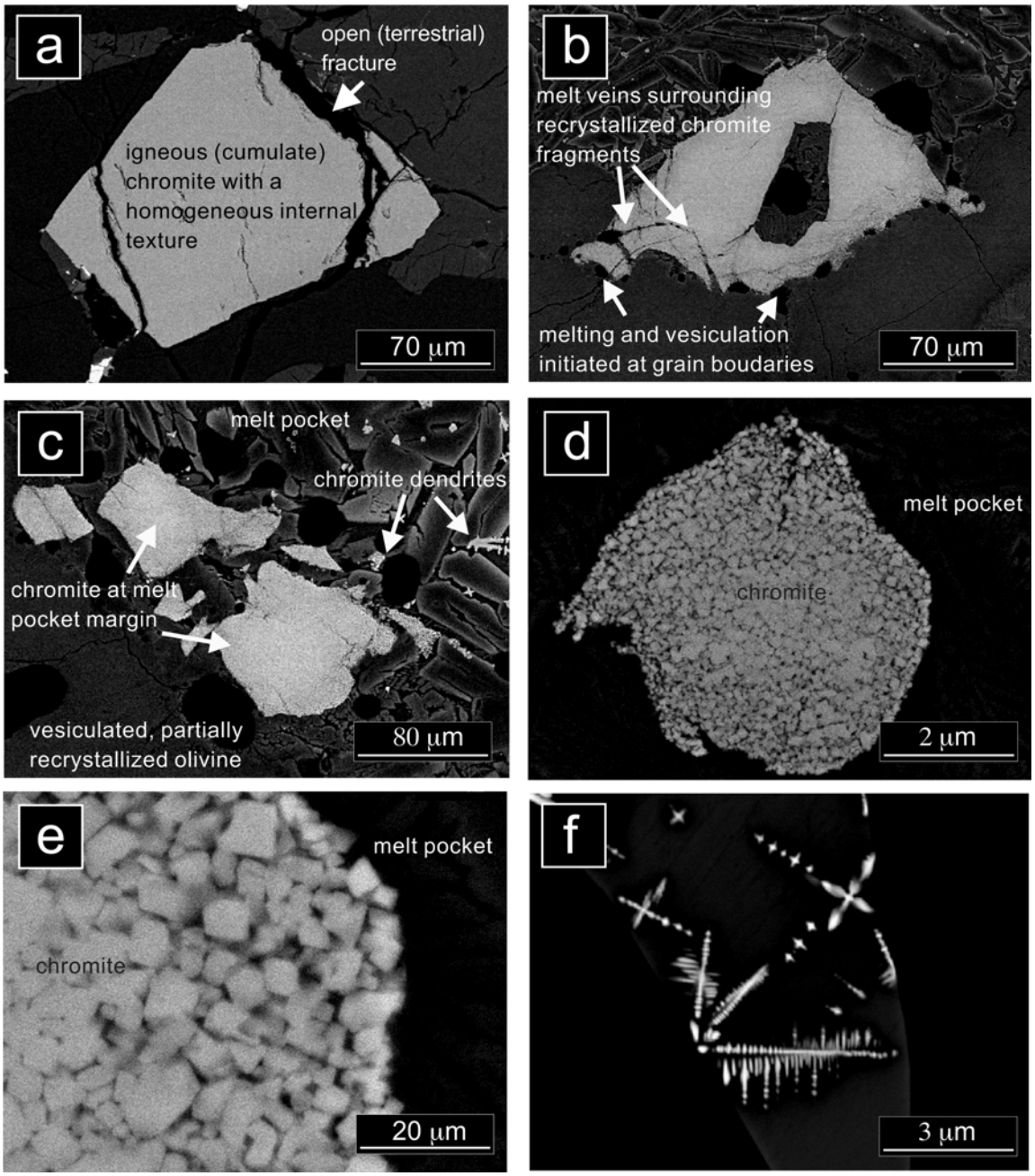


Fig. 8. BSE images showing the various chromite textures in ALH 77005. a) cumulate chromite in non-poikiltiic area showing a euhedral shape and homogeneous texture. b) Chromite grain in direct contact with the melt pocket. The side in contact with host rock olivine shows vesiculation and reaction at the grain boundary, however the overall shape of the original grain is maintained. c) Chromite near the melt pocket margin with a recrystallized rim in direct contact with the melt pocket and a homogeneous internal texture. d) Chromite completely entrained within the melt pocket has a completely recrystallized texture, shown at higher magnification in (e), maintaining the original grain shape. f) Chromite dendrites in melt pocket center.

exhibits incompatible behavior and analyses from melt pocket olivine falls along the same trends as host rock (cumulate and granular) olivine. Cr_2O_3 abundances are much higher in melt pocket crystallites (0.12–0.68 wt% Cr_2O_3) compared to host rock (cumulate) olivine (0.01–0.08 wt% Cr_2O_3) and show a positive correlation with increasing mg-number. Near vertical trends are observed at the highest mg-numbers ($Fo_{85–89}$).

Host rock and melt pocket chromite compositions in ALH 77005 are compared in Fig. 11. Similar to NWA 1950, the compositions of the mottled, recrystallized chromite grains near the melt pocket margins overlap the compositions of chromite grains in the host rock, reflecting a textural, as opposed to compositional, change. In contrast, the chromite dendrites from melt pocket cores extend to more magnesian

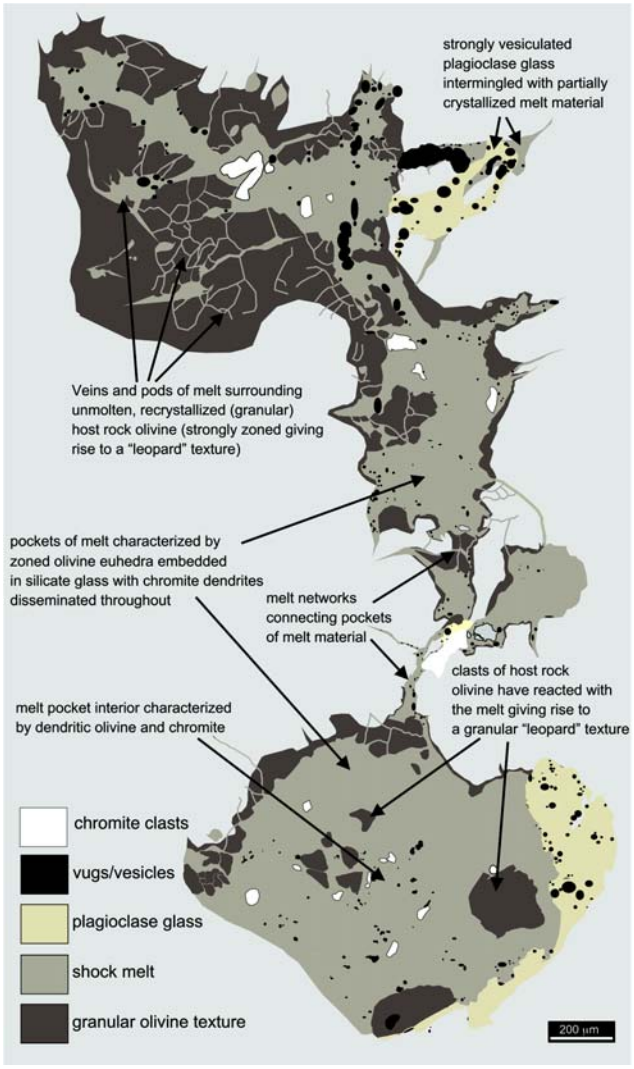


Fig. 9. Sketch of melt pocket networks in ALH 77005 illustrating the relationship between host rock, granular textures, and melt pockets.

and aluminous compositions than those in the host rock; they have Cr# (= molar Cr/(Cr + Al)) as low as 0.6, and Fe# (= molar Fe/(Fe + Mg) as low as 0.53 (cf. host rock Fe# > 0.64).

Equilibration Shock Pressure of Northwest Africa 1950

Although a quantitative measurement (i.e., refractive index of maskelynite; Fritz et al. 2005) of the peak shock pressure recorded in NWA 1950 is lacking, it can be estimated based on observed shock effects in plagioclase (complete transformation to maskelynite), olivine (planar fractures and strong mosaicism) and clinopyroxene (strong mosaicism) (this study; Gillet et al. 2005; Mikouchi 2005). Shock effects vary with increasing shock intensity such that a progression of characteristic stages of shock metamorphism can be recognized and arranged in order of increasing degree of deformation and alteration of the constituent mineral phases. Thus, a shocked rock can be assigned to a shock stage that is not dependent on measurement of the absolute shock pressure, but relative to an existing shock recovery database. Shock recovery experiments and subsequent analysis of the experimentally shocked sample have been performed on single crystal olivine, pyroxene, oligoclase, dunite and polycrystalline olivine, particulate dunite, granulated basalt, lunar regolith, olivine- and pyroxene-bearing basalts, and pyroxenite, particulate enstatite and enstatite-plagioclase mixtures (see Stöffler et al. 1991 for compiled database). The peak shock pressure of NWA 1950, based on these lines of evidence (maskelynite, mechanical deformation of olivine and clinopyroxene), can be estimated at ~35–45 GPa, which corresponds to the strongly shocked S5 shock stage of Stöffler et al. (1991).

Cooling History from Olivine Crystal Shapes in Melt Pockets

Crystal Growth

The strong zoning of dendritic and euhedral olivine crystals, coupled with the observation that textures vary between melt pockets of different sizes, and within individual melt pockets (from melt pocket core to the contact with relatively cold host rock, i.e., a zone of high thermal gradient), indicates that the crystallites formed by diffusion-limited growth from a silicate melt, rather than by devitrification of glasses. Diffusion-limited growth, as the name implies, arises when the kinetics of crystallization are rapid with respect to rates of chemical diffusion, giving rise to a branching texture (Keith and Padden 1963; Dowty 1980). For crystallites formed by secondary devitrification of glasses (i.e., crystallization below the glass transition temperature), textures would not be expected to show a relationship to cooling contacts. In addition, if the dendrites result from devitrification they would be expected to show a relationship to any free surface, i.e., (terrestrial) open, calcite-filled fractures which cut across the melt pockets (Lofgren 1980). Instead, the melt pocket center is characterized by dendritic and/or hopper crystal shapes, progressing to equant euhedra as the contact with the host rock is approached (Figs. 3, 7, and 8).

Heterogeneous Nucleation

Nucleation and subsequent growth of a crystal can either be classified as homogeneous, if it arises entirely through random aggregations of atoms formed due to local, transient supersaturation in the liquid, or heterogeneous, if the presence of another phase (i.e., crystal or gas bubble), in contact with the liquid, facilitates growth (Dowty 1980). The importance of heterogeneous nucleation on the development of texture has been demonstrated for a wide variety of rock types, including, but not limited to, impact melts (Lofgren 1977), terrestrial basaltic rocks (Lofgren 1983), lunar basalts

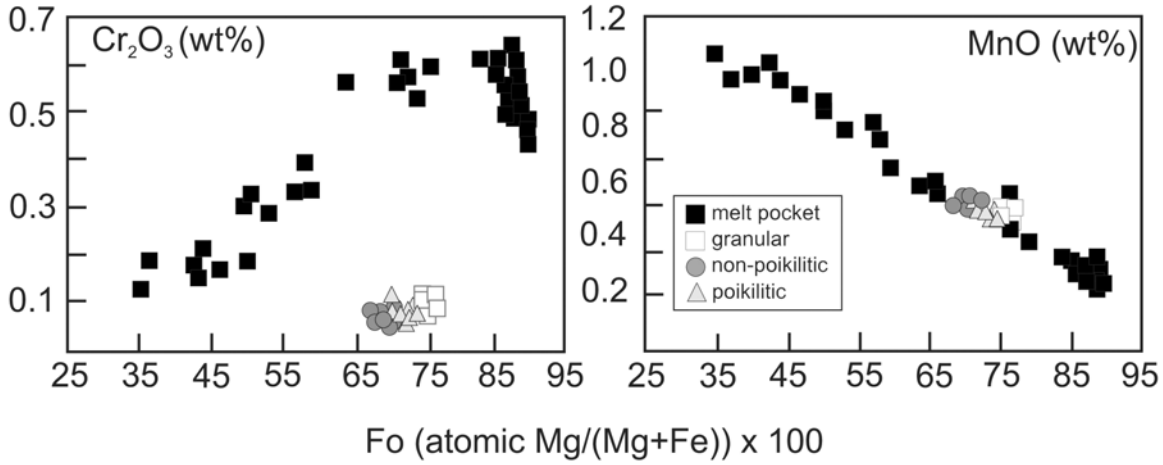


Fig. 10. Variations of Cr_2O_3 and MnO, relative to mg-numbers, in cumulate olivine (poikilitic and non-poikilitic), recrystallized olivine adjacent to melt pocket (granular) and melt pocket crystallites (melt pocket) from ALH 77005.

(Lofgren et al. 1974; Usselman and Lofgren 1976; Bianco and Taylor 1977; Grove and Beaty 1980), and porphyritic pyroxene and olivine chondrules (Lofgren and Russell 1986; Lofgren 1989).

Lofgren (1989) conducted a series of crystallization experiments, designed to assess the effect of heterogeneous nucleation on texture as a function of melting conditions. These experiments show that the heterogeneous nucleation behavior and cooling rate are the prime controlling factors required to reproduce textures from melts of porphyritic olivine chondrule composition. The transition from radial and barred olivine to porphyritic (elongate or equant skeletal to equant euhedral) olivine represents a significant reduction in the number of nucleation sites in the melt at the initiation of cooling. The materials melted to form radial and barred olivine were melted at a higher temperature compared to melts crystallizing porphyritic textures. In melts crystallized to form porphyritic textures, growth is initiated at a smaller degree of undercooling (tens of degrees) compared to melts crystallizing barred crystals. Cooling rates varied from 100 to 1000 °C/hr.

For millimeter-size melt pockets in NWA 1950, a change in crystal shape is observed with distance towards the host rock/melt margin. It should be noted that, although gradational textures are observed from melt pocket to host rock, the melt pocket margin is defined here as the boundary between granular (host rock) and microporphyritic (melt pocket) textures. The melt pocket interior is characterized by randomly oriented dendritic olivine, progressing to a zone of euhedral, equant shapes at the melt pocket margin. Thus, a profile is observed from a zone heated at, or slightly above, the liquidus, where embryos and few nuclei are present at the onset of crystallization, to a zone where preexisting crystalline material survived the melting episode, providing abundant sites for heterogeneous growth. It should be noted that radial and/or barred olivine textures have not been

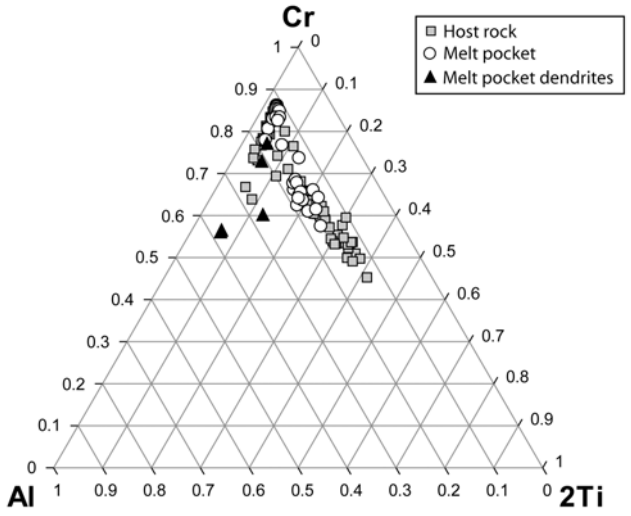


Fig. 11. Compositions of chromites in ALH 77005 in the system chromite (molar Cr/[Cr + 2Ti + Al])-ulvöspinel (molar 2Ti/[Cr + 2Ti + Al])-spinel (molar Al/[Cr + 2Ti + Al]). Melt pocket compositions are those of mottled, recrystallized chromites near melt pocket margins. Melt pocket dendrites are dendritic chromites within melt pocket centers.

observed in this study, thus NWA 1950 and ALH 77005 melt pockets could not have been melted at temperatures significantly above their liquidi for a long period of time (required to destroy all nuclei, preserving only embryos).

We can test this conclusion by comparing the nucleation density (number of nuclei per unit volume) within a melt pocket from margin to center (melt pocket center = apparent melt pocket diameter/2). The nucleation density is measured assuming that each crystal represents a former nucleus. Melt pockets in NWA 1950 show a relationship between crystal shape and nucleation density with distance from the host rock/ melt pocket contact: olivine euhedra near the margin have a nucleation density of 1.6×10^5 crystals/mm^2. Dendritic

crystals, occupying the melt pocket center, have a nucleation density that is two orders of magnitude lower than near margin crystals (1×10^3 crystals/mm^2). The results agree with the interpretation that olivine euhedra crystallizing near the melt pocket margin cooled from a melt containing abundant nuclei while olivine in the melt pocket center cooled from a melt containing few nuclei at the onset of crystal growth. It should be noted that dendrites have been shown to form by repetition in the third dimension of the basic hopper unit (Faure et al. 2003). Thus, the assumption that each dendritic crystal represents a single nucleus may lead to an overestimation of the nucleation density for the melt pocket center only; however, this will not affect the interpretation of melt pocket data.

In the melt pocket center, almost all nuclei were destroyed during the thermal event. Melt times required to eliminate nuclei vary from hours at subliquidus conditions, to seconds to a fraction of a second if liquidus temperatures are exceeded by a significant amount (Lofgren 1989). For melts produced by shock metamorphism, the latter scenario of transient superheating and cooling conditions are favored, rather than a sustained heating event. This is based on crystallization rates of melt pockets determined by crystallization experiments (780–1560 °C/hr; Walton et al. 2006), and the preservation of high pressure polymorphs in some melt pockets attesting to a rapid cooling environment (Beck et al. 2004). Although dendritic and skeletal crystals in the melt pocket center certainly did not form under equilibrium conditions, it is useful to compare the temperatures required to crystallize an olivine of a given composition using equilibrium phase diagrams determined for the Mg_2SiO_4-Fe_2SiO_4 binary system (Bowen and Schairer 1935). A minimum temperature of 1750 °C is required to crystallize an olivine at Fo_{89} (the maximum Mg-number analyzed from a melt pocket crystallite in the center of the melt pocket). The less forsteritic host rock olivine at the melt pocket margin limits the temperature to 1450–1550 °C in order to avoid melting of olivine at $Fo_{68–75}$. It should be noted that temperatures of 1750 °C for the melt pocket center is only a minimum estimate, since the temperature could have been significantly higher, but only for seconds to a fraction of a second, and that this provides only a rough estimate of temperature, since melt pockets do not crystallize under equilibrium conditions.

To preserve crystalline material as nuclei to yield a high density of equant, euhedral crystals, the temperatures near the melt pocket margins must not have been above their liquidi for times exceeding minutes and were likely never above their liquidii. Within the melt pocket, a high thermal gradient must have existed giving rise to an uneven distribution of nuclei at the onset of crystallization. From the temperature estimates discussed previously, assuming a melt pocket diameter of 400 μm (Fig. 3), we calculate a minimum thermal gradient of 1 °C/μm. The cooling rate of these melts was likely on the order of 100–1000 °C/hr (Lofgren 1989). A series of crystallization experiments is required to determine the limits for the melting episode, based on the liquidus temperature of NWA 1950 melt pockets, as well as the dependence of texture on cooling rate.

The internal textures of chromite, entrained within the melt pocket, reflect increasing degrees of recrystallization: chromite grains near the melt pocket margins are recrystallized but retain the composition and outline of the original grains; within the melt pocket center, chromite euhedra and dendrites are present instead, reflecting complete melting and recrystallization. This textural evidence supports the interpretation that strong thermal gradients were present in the melt pocket, giving rise to a heterogeneous distribution of nucleation sites, resulting in gradational textures of olivine upon crystallization.

Melting Martian Rocks by Shock

In Situ Melting Versus an Injection Origin

Localized melting features in Martian meteorites are attributed to shock based on: 1) crosscutting relationships with igneous textures and overprinting by terrestrial alteration (calcite veins, etc.), 2) annealing of mechanical shock defects (planar fractures, mosaicism etc.) in host rock minerals in direct contact with large (millimeter-size) melt pockets, 3) the presence of high-pressure polymorphs (stishovite, hollandite, etc.) in some melt pockets and shock veins, 4) restriction of melt pockets to those Martian meteorites recording mechanical evidence for high bulk shock pressure (~20–55 GPa) and their absence in lightly shocked samples (~5–15 GPa), and 5) the diagnostic signature (in terms of absolute elemental abundances and isotopic ratios) of the Martian atmosphere found in melt pocket of several Martian meteorites (Bogard and Johnson 1983; Bogard et al. 1986; Wiens and Pepin 1988; Bogard et al. 1989; Treiman et al. 1994; Marti et al. 1995; Garrison and Bogard 1999; Beck et al. 2004; Fritz et al. 2005; Walton et al. 2005).

Melting, attributed to a heterogeneous temperature distribution in the bulk rock sample as a result of shock metamorphism, is observed either as planar to sub-planar (shock veins) or sub-spherical (melt pockets) areas of localized melting. Shock veins have been studied more extensively than melt pockets: they have been formed in shock-recovery experiments (Kenkmann et al. 2000; Langenhorst et al. 2002) and friction-welding experiments (Spray 1995; Van der Bogert et al. 2003). In addition, natural analogues have been observed in other meteorite types (Stöffler et al. 1991) and in terrestrial impact structures (Thompson and Spray 1996). The formation conditions of shock veins by slip at high strain rates causing comminution and frictional melting, is thus well constrained from experimental simulation.

The generation of local hot spots (melt pockets and

associated melt veins) is not well understood. This is surprising in light of the fact that the most direct evidence linking these meteorites (shergottites, nakhlites, chassignites, and one orthopyroxenite) to Mars is the large volume of Martian atmosphere measured in shergottite melt pockets (Bogard and Johnson 1983). Possible mechanisms for melt pocket formation include injection of molten material in the vicinity of the target rock during shock, or in situ melting due to shock impedance (shock wave velocity multiplied by the mineral/phase density) contrasts enhanced by pore space within the target (Wiens and Pepin 1988; Bogard et al. 1986, 1988; Stöffler et al. 1991).

The results of this study favor melt pocket formation by in situ melting of host rock constituents by shock. This is based on: 1) gradational textures observed in host rock minerals approaching melt pockets, 2) melt veins, originating from melt pockets, surround unmolten host rock constituents, 3) a positive correlation between vol% shock melts and equilibration shock pressure, and 4) minor element trends in melt pocket crystallites.

In terms of textural evidence, injected melt would be expected to exhibit sharp crosscutting relationships with the host rock, with evidence for forceful injection (i.e., displacement and truncations of host rock minerals). This has been observed in many terrestrial impact structures (Tuchscherer and Spray 2002).

A general relationship between equilibration shock pressure and abundance of shock melting has been established. As shock pressure increases, so does the vol% of shock melt. The nakhlites, shocked to pressures <15 GPa, do not contain melt pockets. The most lightly shocked olivine-phyric shergottite (Yamato 980459, 20–25 GPa; Greshake et al. 2004) is reported to contain rare melt pockets (Mikouchi et al. 2004). Zagami, recording equilibration shock pressures of 29.2 ± 0.6 GPa (Fritz et al. 2005), contains only 1.2 vol% localized melt products (pockets + veins), while more highly shocked meteorites NWA 1950, Los Angeles, DaG 476, SaU 150, and Lewis Hills 88516 (in excess of 35 GPa; Table 1) contain abundant melt products (up to 11.3 vol% for SaU 150). In addition, the observation that melt pockets in meteorites shocked to equilibration pressures 20–45 GPa have self-contained melt pockets while ALH 77005, shocked to the highest equilibration shock levels (45–55 GPa), exhibits extensive melt networks and interconnected melt pockets (Fig. 9). This suggests that ALH 77005 may be transitional between discreet shock melting and bulk rock melting.

Granular olivine adjacent to the melt pocket and entrained clasts overlap in composition with their precursor cumulate olivine grains, representing material recrystallized at subliquidus temperatures, and not remobilized and homogenized. MnO (wt% oxide) shows incompatible behavior in both igneous (cumulate) and melt pocket olivine, reflecting local melting of the host rock olivine. If melt pockets represent injected melt, we would expect to see different MnO contents depending on the nature and origin of the material that was melted.

Further evidence in support of melt pocket formation by in situ melting lies in Cr_2O_3 contents (wt% oxide) in melt pocket olivine. Elevated abundances of Cr_2O_3 are observed for NWA 1950 and ALH 77005 melt pocket olivine crystallites, compared to cumulate olivine. A target rock such as a polycrystalline igneous rock contains heterogeneities such as the various mineral constituents (olivine, pyroxene, plagioclase, chromite, etc.) and vugs (fractures, pore space, etc.). If melt pockets form by shock impedance contrasts, melts would initiate at the grain boundary between phases with contrasting shock impedance (e.g., chromite—an incompressible mineral—and void space). The elevated Cr_2O_3 contents of melt pocket olivine can be explained by preferential melting of chromite in the host rock. Initial crystallization of the melt pocket is marked by high mg-number, Cr-rich olivine dendrites, followed by less magnesian olivine rims and small chromite dendrites or euhedra. Indeed, in shocked ordinary chondrites, Stöffler et al. (1991) observe preferential mobilization of troilite and metal by local melting processes during shock.

Thus, the formation of melt pockets by in situ melting of variable proportions of host rock minerals is consistent with observations of the textural and compositional characteristics of melt pockets.

Origin of Vesicles

The signature of the Martian atmosphere, in terms of relative elemental abundances and isotopic ratios of rare gases, has been found in the melt pockets of several Martian basalts and lherzolitic basalts (Bogard and Johnson 1983; Becker and Pepin 1986; Swindle et al. 1986; Marti et al. 1995; Bogard and Garrison 1999; Walton et al., Forthcoming). Vesicles within melt pockets likely arise from trapped Martian atmospheric gases exsolved as bubbles when shock pressures are relaxed to ambient conditions. Although the rare gas content of the vesicles has not been analyzed directly, we assume that the melt analyzed by step heating and laser probe analyses are in equilibrium with the vesicles.

Spray (1999) proposed cavitation as a mechanism for discreet generation of high-pressure-high-temperature polymorphs in meteorite shock veins and terrestrial impact structures. Cavitation is the rupture of a liquid in response to a decrease in pressure at roughly constant temperature, such that the pressure falls below the saturated vapor pressure. Cavitation includes inception, growth, and collapse of a rupture. In this context, vesicles are regarded as a rupture in the silicate liquid, formed due to rarefaction of the shock wave. Vesicles are thus a decompression effect such that the liquid is subject to conditions of very high pressure to very low pressure, and so ruptures on expansion generating vapor-filled cavities. Some of these cavities may be “frozen in” and preserved before they can collapse and disappear. It is

interesting to note that the cavitated melt would act as a vacuum, and, as the bubbles relaxed to ambient pressures, atmospheric volatiles in the surrounding volume would migrate into the cavity.

In the case of vesiculated plagioclase glass in ALH 77005, previous studies of the noble gas content of maskelynite from grain-separates (Bogard and Garrison 1999), and in situ laser probe analyses (Walton et al., Forthcoming), show that, although melt pockets contain a nearly pure sample of the Martian atmosphere, maskelynite also contains a trapped gas component. It is likely that the vesicles in ALH 77005 plagioclase glass, like the melt pockets, represent exsolved Martian atmospheric gases.

Ejection of Martian Rocks

Various impact scenarios have been proposed as a mechanism to accelerate Martian surface or near surface material in excess of 5.0 km/s (Mars' escape velocity; Wetherill 1984). Modes for ejection mechanisms involve theoretical investigation by numerical simulations and are evaluated by studying the physical conditions recorded in Martian material that eventually makes its way to Earth for study after residence times of generally a few million years in space (e.g., Fritz et al. 2005; see also Nyquist et al. 2001 for compiled CRE ages). The spallation ejection mechanism, whereby solid material is accelerated at high velocity by stress wave interference (Melosh 1984, 1985), has been supported by laboratory shock recovery experiments of Gratz et al. (1993) and is most consistent with shock effects recorded in Martian meteorites (Fritz et al. 2005). The result is a zone in which the pressure gradient, and not the absolute pressure, is extremely high.

The geochemical characteristics of NWA 1950 as well as CRE age (Gillet et al. 2005) are similar to and overlap with (in the case of CRE age) those properties reported for other lherzolitic shergottites. This indicates that NWA 1950 originated from the same area of the Martian subsurface. Despite a common origin, NWA 1950 is shocked to a lesser degree than ALH 77005 in terms of equilibration shock pressure. This is based on the observation that NWA 1950 plagioclase has been completely converted to a diaplectic glass (maskelynite) whereas ALH 77005 plagioclase quenched to a normal plagioclase glass. Diaplectic glass is formed within a certain pressure range (30–45 GPa), the upper temperature limit of which is determined by the magnitude of post-shock temperature (i.e., the amount of waste heat in the decompressed shocked material). A diaplectic glass is formed while shock pressures are still high (30–45 GPa), through a solid to glass transition, without going through the liquid state (e.g., Quentin and Jeanloz 1989). At higher shock pressure (>45 GPa), the post-shock temperature is high enough so the material is in a liquid state after pressure release to quench a normal glass from a low-pressure liquid (i.e., a glass formed from a liquid to glass transition). In the context of a spallation model for Martian meteorite ejection, this places NWA 1950 near to ALH 77005 but at a shallower depth within the high-pressure gradient that exists within the interference zone during impact. This is consistent with the interpretations of Mikouchi (2005) that NWA 1950 and other lherzolitic shergottites originated from the same igneous body on Mars and were ejected by the same impact event, and that NWA 1950 is intermediate to ALH 77005 and LEW 88516 in terms of igneous re-equilibration during cooling, and therefore intermediate in vertical position within the magma body.

CONCLUSIONS

Based on investigation of the shock metamorphic features recorded in NWA 1950 during ejection from the Martian subsurface, it is concluded that:

- Shock damage is manifested as mechanical deformation and complete transformation of plagioclase to maskelynite in the bulk rock and localized areas of melting and recrystallization (pockets and veins).
- In terms of equilibration shock pressure, NWA 1950 is less highly shocked than ALH 77005, in the range 35–45 GPa.
- The mineral assemblage crystallized from melt pockets is more refractory than cumulate minerals and can be distinguished in terms of mg-number and minor element abundances.
- Heterogeneous nucleation behavior is a controlling factor giving rise to a variety of melt pocket textures.
- Melt pockets arise from in situ shock melting of host rock constituents.
- Vesicles within melt pockets likely arise from trapped Martian atmospheric gases exsolved as bubbles.
- NWA 1950 originated from the same area of the Martian subsurface, but at a shallower depth, compared to ALH 77005.

Acknowledgments–This work has been funded by the Natural Sciences and Engineering Research Council of Canada (NSERC), the Canadian Space Agency and the Alberta Ingenuity Fund through grants awarded to E. L. W. and NSERC Discovery Grant 261740-03 to C. D. K. H. The NWA 1950 tile was purchased for the University of Alberta using funds from the Department of Earth and Atmospheric Sciences. Helpful discussions with Simon Kelley and John Spray on vesicle formation in shock melts are greatly appreciated. Thanks to Ancel Murphy and Calvin Nash at the University of New Brunswick for preparing the NWA 1950 tile for study. Thanks to Sergei Matveev for EM assistance and George Braybrook for FE-SEM assistance. Reviews of an earlier version of this manuscript by T. Mikouchi and an anonymous reviewer are gratefully acknowledged.

Editorial Handling—Dr. Edward Scott

REFERENCES

Artemieva N. and Ivanov B. 2004. Launch of Martian meteorites in oblique impacts. *Icarus* 171:84–101.

Bauer J. F. 1979. Experimental shock metamorphism of mono- and polycrystalline olivine—A comparative study. Proceedings, 10th Lunar and Planetary Science Conference. pp. 2573–2596.

Beck P., Gillet Ph., Gautron L., Daniel I., and El Goresy A. 2004. A new natural high-pressure (Na,Ca)-hexaluminosilicate [$(Ca_xNa_{1-x})Al_{3+x}Si_{3-x}O_{11}$] in shocked Martian meteorites. *Earth and Planetary Science Letters* 219:1–12.

Beck P., Barrat J. A., Gillet Ph., Wadhwa M., Franchi I. A., Greenwood R. C., Bohn M., Cotten J., Van de Moortèle B., and Reynard A. 2006. Petrography and geochemistry of the chassignite Northwest Africa 2737 (NWA 2737). *Geochimica et Cosmochimica Acta* 70:2127–2139.

Becker R. H. and Pepin R. O. 1986. The case for a Martian origin of the shergottites: Nitrogen and noble gases in EETA79001. *Earth and Planetary Science Letters* 69:225–242.

Bianco A. S., and Taylor L. A. 1977. Applications of dynamic crystallization studies: Lunar olivine normative basalts. Proceedings, 8th Lunar Science Conference. pp. 1593–1610.

Boctor N. Z., Fei Y., Bertka C. M., Alexander C. M. O'D., and Hauri E. 1999. Shock metamorphic effects in Martian meteorite ALH 77005 (abstract #1628). 30th Lunar and Planetary Science conference. CD-ROM.

Bogard D. D. and Johnson P. 1983. Martian gases in an Antarctic meteorite? *Science* 221:651–654.

Bogard D. D., Johnson P., and Nyquist L. E. 1984. Cosmic ray exposure of SNC achondrites and constraints on their derivation from Mars (abstract). 15th Lunar and Planetary Science Conference. pp. 68–69.

Bogard D. D., Hörz F., and Johnson P. H. 1986. Shock-implanted noble gases: An experimental study with implications for the origin of Martian gases in shergottite meteorites. *Journal of Geophysical Research* 91:E99–E114.

Bogard D. D., Hörz F., and Johnson P. 1989. Shock-implanted noble gases II: Additional experimental studies and recognition in naturally shocked terrestrial materials. *Meteoritics* 24:113–123.

Bowen N. L. and Schairer J. F. 1935. The system, MgO-FeO-SiO_2. *American Journal of Science* 29:151–217.

Bunch T. W., Irving A. J., Wittke J. H., and Kuehner S. M. 2005. NWA 2646: A Martian plagioclase-olivine clinopyroxenite akin to "lherzolitic shergottites" (abstract #5209). *Meteoritics & Planetary Science* 40:A25.

Clayton R. N. and Mayeda T. K. 1996. Oxygen isotopic studies of achondrites. *Geochimica et Cosmochimica Acta* 60:1999–2017.

Coleman L. C. 1977. Ringwoodite and majorite in the Catherwood meteorite. *Canadian Mineralogist* 15:97–101.

Donaldson C. H. 1976. An experimental investigation of olivine morphology. *Contributions to Mineralogy and Petrology* 57: 187–213.

Dowty E. 1980. Crystal growth and nucleation theory and the numerical simulation of igneous crystallization. In *Physics of magmatic processes*. Princeton: Princeton University Press. pp. 419–485.

Eugster O., Weigel A., and Polnau E. 1996. Two different ejection events for basaltic shergottites QUE 94201, Zagami and Shergotty (2.6 Ma) and lherzolitic shergottites LEW 88516 and ALHA77005 (3.5 Ma) (abstract). 28th Lunar and Planetary Science Conference. pp. 345–346.

Eugster O. and Polnau E. 1997. Mars-Earth transfer times of lherzolite Yamato-793605. *Antarctic Meteorite Research* 10: 141–149.

Faure F., Trolliard G., Nicollet C., and Motel J.-M. 2003. A developmental model of olivine morphology as a function of the cooling rate and the degree of undercooling. *Contributions to Mineralogy and Petrology* 145:251–263.

Franchi I. A., Wright I. P., Sexton A. S., and Pillinger C. T. 1999. The oxygen isotopic composition of Earth and Mars. *Meteoritics & Planetary Science* 34:657–661.

Fritz J., Artemieva N., and Greshake A. 2005. Ejection of Martian meteorites. *Meteoritics & Planetary Science* 40:1393–1411.

Garrison D. H. and Bogard D. D. 1999. Isotopic composition of trapped and cosmogenic noble gases in several Martian meteorites. *Meteoritics & Planetary Science* 33:721–736.

Gillet Ph., Barrat J. A., Beck P., Marty B., Greenwood R. C., Franchi I. A., Bohn M., and Cotten J. 2005. Petrology, geochemistry, and cosmic-ray exposure age of lherzolitic shergottite Northwest Africa 1950. *Meteoritics & Planetary Science* 40:1175–1184.

Gleason J. D., Kring D. A., Hill D. H., and Boynton W. V. 1997. Petrography and bulk chemistry of Martian lherzolite LEW 88516. *Geochimica et Cosmochimica Acta* 18:4007–4014.

Goodrich C. A., Herd C. D. K., and Taylor L. A. 2003. Spinels and oxygen fugacity in olivine-phyric and lherzolitic shergottites. *Meteoritics & Planetary Science* 38:1773–1792.

Gratz A. J., Nellis W. J., and Hinsey N. A. 1993. Observations of high-velocity, weakly shocked ejecta from experimental impacts. *Nature* 363:522–524.

Greshake A., Fritz J., and Stöffler D. 2004. Petrology and shock metamorphism of the olivine-phyric shergottite Yamato-980459: Evidence for a two-stage cooling and a single-stage ejection history. *Geochimica et Cosmochimica Acta* 68:2359–2377.

Grove T. L. and Beaty D.W. 1980. Classification, experimental petrology, and possible volcanic histories of the Apollo 11 high-K basalts. Proceedings, 11th Lunar and Planetary Science Conference. pp. 149–177.

Harvey R. P., Wadhwa M., McSween H. Y., Jr., and Crozaz G. 1993. Petrography, mineral chemistry, and petrogenesis of Antarctic shergottite LEW 88516. *Geochimica et Cosmochimica Acta* 57: 4769–4783.

Head J. N., Melosh H. J., and Ivanov B. A. 2002. Martian meteorite launch: High-speed ejecta from small craters. *Science* 298:1725–1756.

Hsu W., Guan Y., Wang H., Leshin L. A., Wang R., Zhang W., Chen X., Zhang E., and Lin C. 2004. The lherzolitic shergottite Grove Mountain 99207: Rare earth element geochemistry. *Meteoritics & Planetary Science* 39:701–709.

Ikeda Y. 1997. Petrology and mineralogy of the Y-793605 Martian meteorite. *Antarctic Meteorite Research* 10:13–40.

Katsura T., Yamada H., Nishikawa O., Song M., Kubo A., Shinmei T., Yokoshi S., Aizawa Y., Yoshino T., Walter J., and Ito E. 2004. Olivine-wadsleyite transition in the system $(Mg,Fe)_2SiO_4$. *Journal of Geophysical Research* 109, doi: 10.1029/2003JB002438.

Keith H. D. and Padden F. J., Jr. 1963. A phenomenological theory of spherulite crystallization. *Journal of Applied Physics* 34: 2409–2421.

Kenkmann T., Stöffler D., and Hornemann U. 2000. Formation of shock-induced pseudotachylites along lithological interfaces. *Meteoritics & Planetary Science* 35:1275–1290.

Langenhorst F., Poirier J.-P., Deutsch A., and Hornemann U. 2002. Experimental approach to generate shock veins in single crystal olivine by shear melting. *Meteoritics & Planetary Science* 37: 1541–1553.

Lin Y., Guan Y., Wang D., Kimura M., and Leshin L. A. 2005. Petrogenesis of the new lherzolitic shergottite Grove Mountains 99027: Constraints of petrography, mineral chemistry, and rare earth elements. *Meteoritics & Planetary Science* 40:1599–1619.

Lofgren G., Donaldson C. H., Williams R. J., Mullins O., Jr., and Usselman M. 1974. Experimentally reproduced textures and minerals chemistry of Apollo 15 quartz normative basalts. Proceedings, 5th Lunar Science Conference. pp. 549–567.

Lofgren G. E. 1977. Dynamic crystallization experiments bearing on the origin of textures in impact-generated liquids. Proceedings, 8th Lunar Science Conference. pp. 2079–2095.

Lofgren G. 1980. Experimental studies on the dynamic crystallization of silicate melts. In *Physics of magmatic processes*. Princeton:Princeton University Press. pp. 487–551.

Lofgren G. E. 1983. Effect of heterogeneous nucleation on basaltic textures: A dynamic crystallization study. *Journal of Petrology* 24:229–255.

Lofgren G. and Russell W. J. 1986. Dynamic crystallization of chondrule melts of porphyritic and radial pyroxene composition. *Geochimica et Cosmochimica Acta* 50:1715–1726.

Lofgren G. 1989. Dynamic crystallization of chondrule melts of porphyritic olivine composition: Textures experimental and natural. *Geochimica et Cosmochimica Acta* 53:461–470.

Marti K., Kim J. S., Thakur A. N., McCoy T. J., and Keil K. 1995. Signatures of the Martian atmosphere in glass of the Zagami meteorite. *Science* 267:1983–1984.

Mason B., Nelen J., and White J. S., Jr. 1968. Olivine-garnet transformation in a meteorite. *Science* 160:66–67.

McSween H. Y., Jr., Taylor L. A., and Stolper E. 1979. Allan Hills 77005: A new meteorite type found in Antarctica. *Science* 204: 1201–1203.

Melosh H. J. 1984. Impact ejection, spallation, and the origin of meteorites. *Icarus* 59:234–260.

Melosh H. J. 1985. Ejection of rock fragments from planetary bodies. *Geology* 13:144–148.

Meyer C. 2006. Mars meteorite compendium. http://curator.jsc.nasa.gov/antmet/mmc/index.cfm.

Mikouchi T., Koizumi E., McKay G., Monkawa A., Ueda Y., Chokai J., and Miyamoto M. 2004. Yamato-980459: Mineralogy and petrology of a new shergottite-related rock form Antarctica. *Antarctic Meteorite Research* 17:13–34.

Mikouchi T. 2005. Northwest Africa 1950: Mineralogy and comparison with Antarctic lherzolitic shergottites. *Meteoritics & Planetary Science* 40:1621–1634.

Mittlefehldt D. W. 1994. ALH 84001, a cumulate orthopyroxenite member of the Martian meteorite clan. *Meteoritics* 29:214–221.

Miura Y. N., Nagao K., Sugiura N., Sagawa H., and Matsubara K. 1995. Orthopyroxenite ALH 84001 and shergottite ALHA77005: Additional evidence for a Martian origin from noble gases. *Geochimica et Cosmochimica Acta* 59:2105–2113.

Nagao K., Nakamura T., Muira Y. N., and Takaoka N. 1997. Noble gas studies and mineralogy of primary igneous material of the Yamato-793605 shergottite. *Antarctic Meteorite Research* 10: 125–142.

Nagao K., Nakamura T., Okazaki R., Miura Y. N., and Takaoka N. 1998. Two stage irradiation of the Y-793605 Martian meteorite (abstract). *Meteoritics & Planetary Science* 33:A114.

Nishiizumi K., Klein J., Middleton R., Elmore D., Kubnik P. W., and Arnold J. R. 1986. Exposure history of shergottites. *Geochimica et Cosmochimica Acta* 50:1017–1021.

Ostertag R., Omthauer G., Rager H., and McSween H. Y., Jr. 1984. Fe^{3+} in shocked olivine crystals of the ALH 77005 meteorite. *Earth and Planetary Science Letters* 67:162–166.

Pal D. K., Tuniz C., Moniot R. K., Savin W., Druse T., and Herzog G. F. 1986. Beryllium-10 contents of shergottites, nakhlites, and Chassigny. *Geochimica et Cosmochimica Acta* 50:2405–2409.

Quentin W. and Jeanloz R. 1989. Static amorphization of anorthite at 300 K and comparison with diaplectic glass. *Nature* 338:413–415.

Reimold W. U. and Stöffler D. 1978. Experimental shock metamorphism of dunite. Proceedings, 9th Lunar and Planetary Science Conference. pp. 2805–2824.

Reynard B., Van de Mootele B., Beck P., and Gillet P. 2006. Shock-induced transformations in olivine of the chassignite NWA 2737 (abstract #1837). 37th Lunar and Planetary Science Conference. CD-ROM.

Russell S. S., Folco L., Jones R., Grady M. M., Zolensky M. E., Righter K., Zipfel J., and Grossman J. N. 2004. The Meteoritical Bulletin, No. 88. *Meteoritics & Planetary Science* 39:A215–A272.

Russell S. S., Zolensky M. E., Righter K., Folco L., Jones R., Connolly H. C., Grady M. M., and Grossman J. N. 2005. The Meteoritical Bulletin, No. 89. *Meteoritics & Planetary Science* 40:A201–A263.

Spray J. G. 1995. Pseudotachylyte controversy: Fact or friction? *Geology* 23:1119–1122.

Spray J. G. 1999. Shocking rocks by cavitation and bubble implosion. *Geology* 27:695–698.

Stöffler D., Keil K., and Scott E. R. D. 1991. Shock metamorphism of ordinary chondrites. *Geochimica et Cosmochimica Acta* 55: 3845–3867.

Swindle T. D., Caffee M. W., and Hohenberg C. M. 1986. Xenon and other noble gases in shergottites. *Geochimica et Cosmochimica Acta* 55:3845–3867.

Terribilini D., Eugster O., Burger M., Jakob A., and Krahenbuhl U. 1998. Noble gases and chemical composition of Shergotty mineral fractions, Chassigny, and Yamato-793605: The trapped argon-40/argon-36 ratio and ejection times of Martian meteorites. *Meteoritics & Planetary Science* 33:677–684.

Thompson L. M. and Spray J. G. 1996. Pseudotachylyte petrogenesis: Constraints from the Sudbury impact structure. *Contributions to Mineralogy and Petrology* 125:359–374.

Treiman A. H., McKay G. A., Bogard D. D., Wang M.-S., Lipschutz M. E., Mittlefehldt D. W., Keller L., Lindstrom M. M., and Grady M. M. 1994. Comparison of LEW 88516 and ALHA77005 Martian meteorites: Similar but distinct. *Meteoritics* 29:581–592.

Tuchscherer M. G. and Spray J. G. 2002. Geology, mineralization, and emplacement of the Foy Offset Dike, Sudbury impact structure. *Economic Geology and the Bulletin of the Society of Economic Geologists* 97:1377–1397.

Usselman T. M. and Lofgren G. E. 1976. The phase relations, textures, and mineral chemistries of high-titanium mare basalts as a function of oxygen fugacity and cooling rate. Proceedings, 7th Lunar Science Conference. pp. 1345–1363.

Van der Bogert, C. H., Schultz P. H., and Spray J. G. 2003. Impact-induced frictional melting in ordinary chondrites: A mechanism for deformation, darkening, and vein formation. *Meteoritics & Planetary Science* 38:1521–1532.

Walton E. L., Spray J. G., and Bartoschewitz R. 2005. A new Martian meteorite from Oman: Mineralogy, petrology, and shock metamorphism of olivine-phyric basaltic shergottites Sayh al Uhaymir 150. *Meteoritics & Planetary Science* 40:1195–1214.

Walton E. L., Shaw C. S., Cogswell S., and Spray J. G. 2006. Crystallization rates of shock melts in three Martian basalts: experimental simulation with implications for meteorite launch diameters. *Geochimica et Cosmochimica Acta* 70:1059–1075.

Walton E. L., Kelley S. P., and Spray J. G. Forthcoming. Shock implantation of Martian atmospheric argon in four basaltic shergottites: A laser probe $^{40}Ar/^{39}Ar$ investigation. *Geochimica et Cosmochimica Acta*.

Wiens R. C. and Pepin R. O. 1988. Laboratory shock emplacement of noble gases nitrogen, and carbon dioxide into basalt, and implications for trapped gases in shergottite EETA79001. *Geochimica et Cosmochimica Acta* 52:295–307.

Wetherill G. W. 1984. Orbital evolution of impact ejecta from Mars. *Meteoritics* 19:1–13.